Estimating Land Surface All-Wave Daily Net Radiation From VIIRS Top-of-Atmosphere Data

Xiuwan Yin, Bo Jiang, Yingping Chen, Yu Zhao, Xiaotong Zhang, Yunjun Yao, Xiang Zhao, and Kun Jia

***Abstract*— Be aware of the significance of land surface net radiation (R_n), there is a need for accurate long-term and high spatial resolution global R_n estimates based on satellite data. Herein, we propose a novel globally applicable, highly effective algorithm for estimating daily R_n directly from Visible Infrared Imaging Radiometer Suite (VIIRS) top-of-atmosphere (TOA) observations ranging from 2011 to present, using the eXtreme Gradient Boosting (XGBoost) method. This algorithm, named the constraint conditional model (CCM), consists of five conditional models (namely, cases 1–5 model) divided by the combination of the length of daytime (dt), the instantaneous sky condition, and the surface broadband albedo, and the daily downward shortwave radiation (DSR) from ERA5-Land was introduced as a physical constraint when $dt > 9$, in which case R_n is dominated by R_{si} (incoming solar radiation). The validation accuracy of CCM was satisfactory against the ground measurements, yielding a root-mean-square error (RMSE) of 18.95 Wm^{-2}, a bias of 0.056 Wm^{-2}, and an R^2 of 0.89. The algorithm exhibited superior accuracy and robustness compared to GLASS-MODIS and ERA5-Land under spatiotemporally independent validation samples. This indicates the potential of VIIRS to extent MODIS R_n products for generating long-term global daily R_n data.**

***Index Terms*— ERA5-Land, eXtreme gradient boosting (XGBoost), GLASS-MODIS, modeling, net radiation, Visible Infrared Imaging Radiometer Suite (VIIRS).**

I. Introduction

LAND surface all-wave net radiation (R_n) characterizes the available radiative energy budget over land surface. R_n is the algebraic sum of the from the shortwave (0.3–3.0 μm) to the longwave (3.0–100.0 μm) portions of the electromagnetic spectrum [1], [2] and is mathematically expressed as

$$R_n = (1 - \alpha)R_{si} + (R_{li} - R_{lo}) \tag{1}$$

where R_{si} is the surface incoming solar radiation, α is the surface broadband shortwave albedo, and R_{li} and R_{lo} are the surface downward and upward longwave radiation, respectively. The units for all radiative components are Wm^{-2} and downward is defined as positive. R_n controls the energy exchange and drives most physical and biological processes on the Earth, such as evapotranspiration and photosynthesis, among others. Thereby, R_n is also one of the most essential parameters in land surface, hydrological, and ecological models. Therefore, accurate R_n observations or estimates are highly required for various applications and studies.

Due to various limitations in the ground measurements [3], satellite-based R_n estimates, especially those derived from the polar-orbiting satellites (i.e., GLASS<Global Land Surface Satellite>-MODIS [2], [4] and CERES SYN series <Clouds and the Earth's Radiant Energy System-Synoptic>), are more popular because of their superior performance [3], [5]. However, MODIS, one of the most widely used satellite data during the past two decades, is set to be replaced by the Visible Infrared Imaging Radiometer Suite (VIIRS). VIIRS is a replaced sensor onboard the Suomi National Polar-orbiting Partnership (SNPP) satellite launched on October 28, 2011, providing products (e.g., VNP02MOD, VNP03MOD, and CLDMSK) at 375-/750-m spatial resolution with the similar band settings as MODIS [6]. As being regarded as the extension of MODIS to ensure the long-term continuity of environmental data records (EDRs), VIIRS data have been applied to estimate various parameters, such as shortwave radiation [7], upward longwave radiation [8], leaf area index (LAI) [9], and albedo [10]. However, VIIRS has not released any radiative products so far, especially for R_n.

Recently, satellite-based estimation algorithms that directly estimate R_n from top-of-atmosphere (TOA) observations (hereinafter TOA-based algorithm) have attracted more attention [11], [12]. The TOA-based algorithm, first proposed by Wang et al. [13], used MORTRAN simulations and combined visible and shortwave infrared (VSWIR) and thermal infrared (TIR) remote sensing data with the linear regression method. Afterward, machine learning (ML) has led to a surge in TOA-based R_n estimation algorithms. Chen et al. [14] developed a model with the genetic algorithm and artificial neural network (GA-ANN) to estimate daily R_n at high latitudes from MODIS TOA bands, demonstrating its superiority to the estimates from CERES. Be inspired by this work, Li et al. [15] developed a new model with random forest (RF) to estimate daily R_n at mid-low latitudes from MODIS TOA observations. It introduced the ERA5 daily R_n as a physical constraint [16] to address the challenge of insufficient information provided by MODIS TOA observations in the mid-low latitudes. Similarly, this estimation framework was improved by Xu et al. [17] to

Manuscript received 4 January 2024; revised 30 May 2024; accepted 6 June 2024. Date of publication 11 June 2024; date of current version 21 June 2024. This work was supported in part by the National Natural Science Foundation of China under Grant 42090012 and Grant 41971291 and in part by the Open Research Program of the International Research Center of Big Data for Sustainable Development Goals under Grant CBAS2022ORP01. *(Corresponding author: Bo Jiang.)*

The authors are with the State Key Laboratory of Remote Sensing Science, Institute of Remote Sensing and Digital Earth, Chinese Academy of Sciences, and the Faculty of Geographical Science, Beijing Engineering Research Center for Global Land Remote Sensing Products, Institute of Remote Sensing Science and Engineering, Beijing Normal University, Beijing 100875, China (e-mail: yinxiuwan@mail.bnu.edu.cn; bojiang@bnu.edu.cn; ypchen01@mail.bnu.edu.cn; yu_zhao@mail.bnu.edu.cn; xtngzhang@bnu.edu.cn; boyyunjun@163.com; zhaoxiang@bnu.edu.cn; jiakun@bnu.edu.cn).

Digital Object Identifier 10.1109/LGRS.2024.3412731

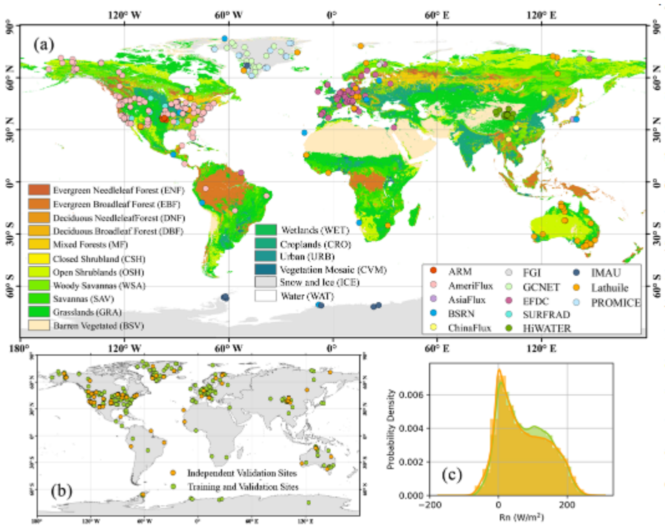

Fig. 1. (a) Spatial distribution of all 413 sites and their land cover types in MCD12Q1. (b) Spatial distribution of the 363 training and validation sites and 50 independent validation sites. (c) Probability density histogram. Note that the characteristics of the independent validation samples were similar to those of the training data.

generate global daily R_n data during 1981–2019 from AVHRR TOA bands constrained by the Modern-Era Retrospective Analysis for Research and Applications (MERRA2) daily R_n [18] with a residual convolutional neural network (RCNN).

Overall, the TOA-based algorithm could estimate R_n theoretically without depending on any high-level products of surface and atmospheric parameters, and the corporation of physical constraints is an effective way to improve its estimation accuracy. Therefore, in this letter, we proposed and validated a globally applicable VIIRS TOA-based daily R_n estimation algorithm with constraints, which consists of five conditional models to fill the study gap in R_n estimates based on VIIRS data.

II. Methodology

A. Datasets

Three kinds of data were used in this study, including ground measurements, remotely sensed data, and ERA5-Land reanalysis data. In situ R_n and R_{si} measurements from 413 sites in 13 global observing networks (2012–2022) were used for model development and validation (Fig. 1). Among these, 50 spatially and temporally independent sites [orange circles in Fig. 1(b)], unused in other product generation, were selected for intercomparison to ensure the spatial independence of validation samples (no. of samples = 40 355). Further details are available in Jiang et al. [5]. All quality-controlled R_n and R_{si} measurements were transferred to local time format first and then aggregated into a daily time scale. Afterward, all the R_n samples (excluding the independent validation samples) were randomly split: 80% for model training (no. of samples = 363 889), and the other 20% for validation (no. of samples = 91 158).

The remotely sensed data include VIIRS TOA bands and the daily R_n and albedo from GLASS-MODIS products. VIIRS has 16 moderate-resolution bands (M-bands) at 750 m (0.402–12.488 μm), five imaging resolution bands (I-bands) at 375 m, and a DND (day/night) band [6], [19]. Herein, three VIIRS

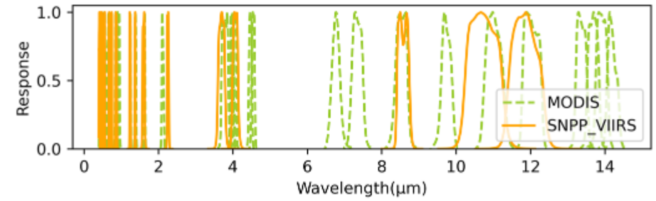

Fig. 2. Comparison in the SRF of VIIRS M-bands (M01–M16) and all of the MODIS bands.

products (https://ladsweb.modaps.eosdis.nasa.gov/missions-and-measurements/viirs/) acquired during 2012–2022, including VNP02MOD (M01-M16 TOA observations), VNP03MOD containing the viewing geometry (i.e., SZA <Solar Zenith Angle>, SAA <Sensor Azimuth Angle>, and VAA <Sensor Azimuth Angle>) and geolocation information (i.e., latitude and elevation), and CLDMSK indicating the sky condition (clear or cloudy) were applied for modeling. Fig. 2 illustrates the comparison in the spectral response function (SRF) of VIIRS and MODIS. The VIIRS M-bands essentially encompass the entire band range of MODIS, except for some water vapor and cloud bands (4.4–8 μm) and infrared bands ($\sim$14 μm). Based on the study of Xu et al. [17], which indicated that the spectral bands up to 12.5 μm could be sufficient for R_n estimation, the VIIRS M01–M16 bands were employed here. Additionally, the VIIRS overpass frequency is about half of that of MODIS and is only daytime, as there is only one rather than two sensors, whereas its swath is wider compared to MODIS.

The GLASS-MODIS daily R_n at 0.05° from 2000 to 2022 (http://glass.umd.edu/NR/Land/) was generated mainly from the GLASS downward shortwave radiation (DSR) product [20] and other ancillary information based on the empirical relationship between R_n and DSR. As the long-term global R_n product with the finest spatial resolution, it was identified as one of the best R_n products [11], performing better than most existing products, and was used for comparison. Additionally, GLASS daily albedo (α) at 0.05° produced based on the angular bin method and statistics-based temporal filtering algorithm with long-term continuity and self-consistency was used for modeling [21].

In this study, the daily DSR from ERA5-Land reanalysis data (https://cds.climate.copernicus.eu/cdsapp#!/dataset/reanalysis-era5-land tab = overview) generated from ECMWF during 2012–2022 was used as the physical constraint [22]. ERA5-Land was generated based on a data assimilation system consisting of an incremental 4-D-Var component for upper-air and near-surface components [23]. Compared to ERA5 [24], ERA5-Land is an enhanced global dataset focusing on land components at a finer spatial resolution (0.1°) covering from 1950 to the present. The accuracy of ERA5-Land daily DSR was also validated against the ground measurements (no. of samples = 435 049), yielding a root-mean-square error (RMSE) of 35.87 Wm^{-2}, which was more accurate than that of GLASS-MODIS (RMSE = 39.12 Wm^{-2}). Besides, the ERA5-Land daily R_n was also used for comparison.

Other ancillary information, including the inverse relative distance from the Earth to the Sun (d_r) and the daytime length (dt), were calculated using the following:

$$d_r = 1 + 0.033 \cos\left(\frac{2\pi \,\text{doy}}{365}\right) \quad (2)$$

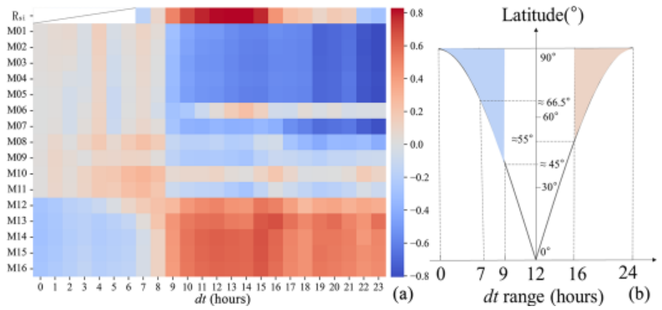

Fig. 3. (a) Correlation between each of the VIIRS TOA observations of M01–M16 and the in situ R_{si} with the in situ R_n for different dt values. (b) Latitudes (south and north) with different dt ranges.

$$dt = \frac{2}{15} * \arccos\left[-\tan(\varphi) * \tan(\text{doy})\right] \tag{3}$$

where φ is the latitude (°) and doy is the day of the year.

B. VIIRS TOA-Based R_n Estimation Algorithm

According to previous studies, R_n is closely linked to R_{si}, and the relationship is determined by dt [5], [14]. Thereby, the optimal TOA bands for the TOA-based algorithm were identified through the correlation between the in situ R_{si} and each of the VIIRS M01–M16 TOA bands with in situ R_n [Fig. 3(a)]. It demonstrated that R_n is closely related to R_{si} when $dt \in$ [9], [16]. The correlation gradually weakened when $dt > 16$. Additionally, shortwave to infrared bands, especially M01–M07 and M12–M16, are also closely related to R_n when $dt \geq 9$. Fig. 3(b) illustrates that $dt > 16$ only at high latitudes (>55°N/S), while $dt \in$ [9], [16] is predominant at mid-low latitudes, consistent with our understanding that R_n is dominated by R_{si} over most regions for most of the time. However, when $dt < 9$, in which case R_n should be dominated by longwave radiation, the correlation between R_n and all bands is not strong. By considering the regions where $dt < 9$ [>45° N/S, Fig. 3(b)] and referring to previous studies, the case was further divided by the combination of α and dt. If $\alpha > 0.7$ or $dt < 7$, which means that the influence of R_{si} on R_n was small, then only the infrared bands were used for calculating R_n, or else all bands would be considered. Accordingly, the flowchart of the VIIRS TOA-based algorithm to estimate daily R_n, named the constraint conditional model (CCM), is designed and shown in Fig. 4.

The uniformity of the conditional model of CCM could be expressed mathematically as

$$R_n = f\left(\text{TOA}_{M_i}, \text{Info}_{j=1,2,\ldots,7}, \text{DSR}^*\right) \tag{4}$$

where TOA_{M_i} is the VIIRS TOA M-bands, $i = 1$–5, 7, 12–16, $\text{Info}_{j=1,2,\ldots,7}$ represents ancillary information, including SZA, VZA, RAA, elevation, d_r, dt, and φ, and DSR^* is the EAR5-Land daily DSR.

As shown in Fig. 4, the daily R_n was estimated from the VIIRS TOA bands separately for five cases. When $dt \in$ [9], [16] with or without cloud at instantaneous times (cases 1 and 2) or $dt > 16$ (case 3), daily R_n was linked with the VIIRS TOA observations of M01–M05, M07, and M12–M16. Conversely, when $dt < 9$, daily R_n was linked with the same bands as in cases 1–3 if $\alpha < 0.7$ and $dt > 7$ (case 4), or else, it was only linked with VIIRS M12–M16 TOA observations (case 5). Moreover, due to the absence of midinfrared bands (~4.5–8 μm, Fig. 2) for capturing atmospheric properties,

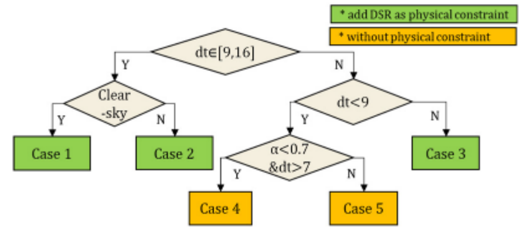

Fig. 4. Flowchart of the VIIRS TOA-based algorithm for daily R_n estimation.

TABLE I
OVERALL VALIDATION ACCURACY OF CCM AND THE MODEL WITHOUT DSR

Overall validation Accuracy	Bias (Wm^{-2})	RMSE (Wm^{-2})	rRMSE (%)	R^2
CCM	0.056	18.95	23.81	0.89
Conditional model without DSR	*−0.087*	*20.95*	*29.70*	*0.91*

limited overpass times at low-mid latitudes (1–4 per day) for characterizing daily atmospheric variations of VIIRS, as well as the strong relationship between R_n and R_{si} when $dt \geq 9$ [Fig. 3(a)], the ERA5-Land daily DSR was introduced as the physical constraint in the DSR-dominated models (cases 1–3).

eXtreme gradient boosting (XGBoost), a powerful boosting model known for its ability to capture nonlinear relationships among inputs and high implementation efficiency [25], has been applied to build the models in the CCM algorithm. XGBoost follows a levelwise strategy, scanning across gradient values and using these partial sums to evaluate the quality of splits at every possible split in the training set. Note that the daily R_n was obtained by averaging all daily R_n estimates of this day if more than one group of TOA observations were available. Additionally, four common statistical measures were used for assessing accuracy: bias, RMSE, relative RMSE (rRMSE), and R^2, among which rRMSE was used to eliminate the influence caused by the different sample sizes.

III. RESULTS AND ANALYSIS

A. Evaluation of the CCM Algorithm

Initially, the overall accuracy of CCM was calculated using all validation samples (91 158 samples). For comparison, the overall accuracy of the five conditional models without DSR was also calculated. Table I indicates that CCM yielded an RMSE of 18.95 Wm^{-2}, a bias of 0.056 Wm^{-2}, and an R^2 of 0.89, showing a reduction in RMSE (rRMSE) by 2 Wm^{-2} (5.89%) compared to that without incorporation of DSR.

Afterward, the validation accuracy of each conditional model for the five cases was computed separately and shown in Table II. The validation accuracy of the model for cases 1–3 but without DSR constraint was also computed for comparison. Overly, the estimation accuracy of CCM for cases 1–3, in which $dt > 9$ and the shortwave radiation dominates R_n, was better than that of cases 4 and 5, yielding the RMSEs of 18.76, 17.92, and 24.84 Wm^{-2}, respectively. Comparatively, CCM significantly improved the estimation accuracy for the three cases after incorporating ERA5-Land daily DSR by reducing their RMSEs of 2.75, 1.48, and 2.17 Wm^{-2} and the magnitudes of bias of 0.445, 0.613, and 0.247 Wm^{-2}, respectively. In particular, the accuracy of case 3 model

TABLE II

VALIDATION ACCURACY OF THE FIVE CONDITIONAL MODELS AND THAT WITHOUT CONSTRAINT IN CASES 1–3

Validation Accuracy	Bias (Wm^{-2})	RMSE (Wm^{-2})	rRMSE (%)	R^2	No. of Samples
case 1	−0.104	18.76	19.64	0.92	50,426
case1 (without DSR)	*−0.549*	*21.51*	*22.52*	*0.89*	
case 2	0.041	17.92	36.75	0.90	17,426
case2 (without DSR)	*0.654*	*19.40*	*39.78*	*0.86*	
case 3	−0.01	24.84	35.88	0.80	8,736
case3 (without DSR)	*0.259*	*26.65*	*41.79*	*0.84*	
case 4	0.378	15.56	85.53	0.47	6,499
case 5	0.135	15.57	87.30	0.46	8,071

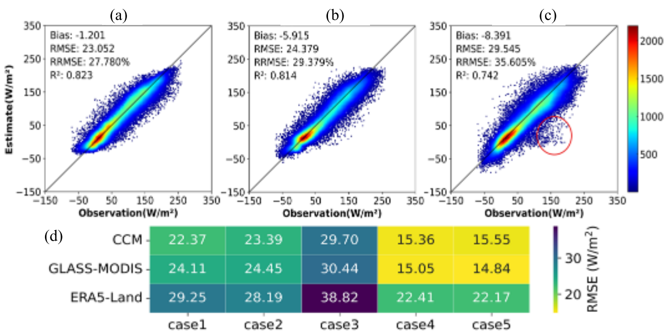

Fig. 5. Overall independent validation accuracy of the daily R_n estimates from (a) CCM, (b) GLASS-MODIS, and (c) ERA5-Land. (d) Performance of the daily R_n estimates from CCM, GLASS-MODIS, and ERA5-Land under cases.

improved the most, with its rRMSE decreasing by 5.89%. This fully demonstrated the effectivity of the introduced DSR in the DSR dominating cases and the strong requirement on the atmospheric information at high latitudes with long daytime duration for the R_n estimation. Cases 4 and 5 mostly appear at high latitudes with a short dt (<9). Their validation accuracy was slightly worse with RMSEs of 15.56 and 15.57 Wm^{-2} and rRMSEs of 85.53% and 87.30%, respectively.

B. Comparison With Other R_n Products

The VIIRS R_n estimates from CCM were compared with the daily R_n from GLASS-MODIS and ERA5-Land using the independent validation samples (shown in Fig. 5). The independent validation accuracy of the CCM R_n estimates was better than that of the two existing R_n products, yielding the smallest RMSE and a bias of 23.052 and −1.201 Wm^{-2}, but its underestimation at high values and overestimation at low values was significant. GLASS-MODIS R_n was in second place, followed by ERA5-Land with their RMSE values of 24.379 and 29.545 Wm^{-2}, respectively. However, they both had the tendency to be underestimated, as indicated by their biases of −5.915 and −8.391 Wm^{-2}. The sparse points of ERA5-Land [red circle in Fig. 5(c)] account for the underestimation caused by ice/snow, similar to ERA5 [11]. Furthermore, the results in Fig. 5(d) were divided into five cases. Comparatively, the accuracy of the CCM R_n estimates was the best for cases 1–3 and was relative worse with that of GLASS-MODIS for cases 4 and 5 due to the deficient in longwave band information. The accuracy of the ERA5-Land daily R_n was the worst for all cases, with an increase in RMSE values by 7–9 Wm^{-2} to other two over the high

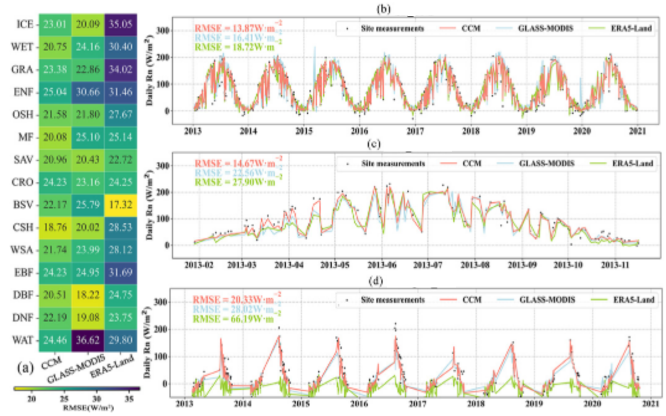

Fig. 6. (a) Performance of daily R_n from CCM, GLASS-MODIS, and ERA5-Land under different land cover types. The time series of the three daily R_n estimates (color lines) and the ground measurements (black points) at three sites. (b) SF_BND (CRO, <40.05°N, 88.37°W>). (c) Lath_CA-Gro (MF, <48.22°N, 80.16°W>). (d) PM-QAS_L (ice/snow, <61.03°N, 46.85°W>).

latitude regions (cases 3–5). These results again illustrated the effectivity of incorporating the ERA5-Land daily DSR as long as the daily R_n was dominated by DSR and also pointed out that more ancillary information is needed to improve the VIIRS R_n estimation accuracy when $dt < 9$. Moreover, ERA5-Land or ERA5 daily R_n at high latitudes should be used with caution.

Additionally, the performance of the three R_n estimates for different land cover types was further examined [Fig. 6(a)]. CCM R_n indicated the most robust performance among the three datasets, with its validated RMSE ranging from 18.76 to 25.04 Wm^{-2}, followed by GLASS-MODIS (18.22–36.62 Wm^{-2}). Specifically, CCM R_n performed the best for WET (20.75 Wm^{-2}), MF (20.08 Wm^{-2}), CSH (18.76 Wm^{-2}), and ENF (25.04 Wm^{-2}), for which the RMSEs were ~4–7 Wm^{-2} lower. However, CCM R_n performed slightly worse than GLASS-MODIS for ICE, DBF, and DNF. Nearly all products performed suboptimally for ENF, with the smallest RMSE values still exceeding 25 Wm^{-2}, consistent with previous findings [11]. Meanwhile, the R_n estimates at three randomly selected sites (SF_BND, Lath_CA-Gro, and PM-QAS_L) were taken as examples. Three R_n estimates varied similarly and closely to the ground measurements at SF_BND [Fig. 6(b)], but the CCM R_n captured the variations in R_n better without any significant outlier value, especially at the ICE site PM-QAS_L [Fig. 6(d)]. ERA5-Land R_n has the tendency to be underestimated, showing relative smooth variations, particularly at the ICE sites as that of ERA5 [11].

Moreover, we examined the spatial mapping ability of CCM. Fig. 7(b) presents the VIIRS daily R_n mapping results by CCM at 750 m on the 270th day of 2021 over southeastern China, which is mostly covered by lush vegetation. For comparison, the daily R_n from GLASS-MODIS (0.05°) and ERA5-Land (0.1°) over the same region is also presented in Fig. 7(c) and (d). These spatial patterns are roughly similar, but the values of GLASS-MODIS are generally higher than those of others by ~10 Wm^{-2}. Comparatively, the CCM R_n could characterize more spatial details than the others because of its finer resolution. Moreover, the running efficiency of CCM is satisfactory as it only takes tens of seconds to produce one swath image of VIIRS.

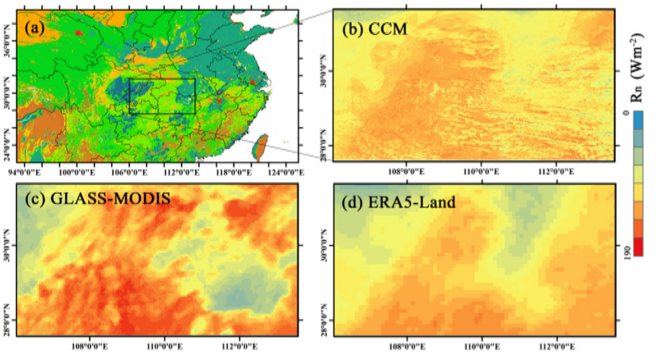

Fig. 7. (a) Land cover over Southeastern China [the legend is the same as in Fig. 1(a)] and the corresponding spatial mapping of daily R_n from (b) CCM, (c) GLASS-MODIS, and (d) ERA5-Land on doy270 of 2021.

IV. Conclusion and Discussion

R_n represents the available surface radiative energy budget and is essential to drive various biophysical processes. However, as the replacement of MODIS, VIIRS has not been used for R_n estimation yet. In this letter, we proposed CCM, a globally applicable, high-efficiency algorithm to estimate the daily R_n from VIIRS TOA M-bands. The algorithm contains five conditional models classified by the combination of dt and α. Additionally, the ERA5-Land daily DSR was introduced as the physical constraint into the DSR dominating models (i.e., cases 1–3) to help provide the required atmospheric information. The estimation accuracy of CCM was satisfactory against ground measurements (RMSE $= 18.95$ Wm^{-2}, bias $= 0.056$ Wm^{-2}, and $R^2 = 0.89$), and its independent validation accuracy (RMSE $= 23.052$ Wm^{-2}, bias $= -1.012$ Wm^{-2}, and $R^2 = 0.832$) was superior to that of GLASS-MODIS and ERA5-Land. Moreover, the performance of the CCM R_n estimates was the most robust under various conditions. However, CCM performed relatively worse at high latitudes when dt was short, which indicates that the VIIRS infrared bands are insufficient to characterize the variations in R_n in this case. Meanwhile, the possible striping issue which is one of the common problems of the tree models XGBoost in mapping should be given more attention. In summary, the new proposed CCM algorithm holds promise for generating accurate global long-term daily R_n products from VIIRS data, extending the data records MODIS continued from the heritage sensors. Hence, addressing the spatiotemporal consistency between daily R_n generated from VIIRS and MODIS is essential for obtaining long-term global R_n products from 2000 to the present in the near future.

Acknowledgment

The authors appreciate the Surface Radiation Budget Network [Fig. 1(a)] offering the field measurements and thank the data support from ECMWF, NASA, and GLASS team.

References

[1] G. Bisht and R. L. Bras, "Estimation of net radiation from the MODIS data under all sky conditions: Southern great plains case study," *Remote Sens. Environ.*, vol. 114, no. 7, pp. 1522–1534, Jul. 2010.

[2] B. Jiang et al., "GLASS daytime all-wave net radiation product: Algorithm development and preliminary validation," *Remote Sens.*, vol. 8, no. 3, p. 222, Mar. 2016.

[3] M. Wild et al., "The energy balance over land and oceans: An assessment based on direct observations and CMIP5 climate models," *Climate Dyn.*, vol. 44, nos. 11–12, pp. 3393–3429, Jun. 2015.

[4] B. Jiang et al., "Empirical estimation of daytime net radiation from shortwave radiation and ancillary information," *Agricult. Forest Meteorol.*, vols. 211–212, pp. 23–36, Oct. 2015.

[5] B. Jiang et al., "The hi-GLASS all-wave daily net radiation product: Algorithm and product validation," *Sci. Remote Sens.*, vol. 7, Jun. 2023, Art. no. 100080.

[6] C. Cao, F. J. De Luccia, X. Xiong, R. Wolfe, and F. Weng, "Early on-orbit performance of the visible infrared imaging radiometer suite onboard the suomi national polar-orbiting Partnership (S-NPP) satellite," *IEEE Trans. Geosci. Remote Sens.*, vol. 52, no. 2, pp. 1142–1156, Feb. 2014.

[7] Y. Zhang, S. Liang, T. He, D. Wang, and Y. Yu, "Estimation of land surface incident and net shortwave radiation from visible infrared imaging radiometer suite (VIIRS) using an optimization method," *Remote Sens.*, vol. 12, no. 24, p. 4153, Dec. 2020.

[8] S. Zhou and J. Cheng, "Estimation of high spatial-resolution clear-sky land surface-upwelling longwave radiation from VIIRS/S-NPP data," *Remote Sens.*, vol. 10, no. 2, p. 253, Feb. 2018.

[9] J. Li, Z. Xiao, R. Sun, and J. Song, "Retrieval of the leaf area index from Visible infrared imaging radiometer suite (VIIRS) surface reflectance based on unsupervised domain adaptation," *Remote Sens.*, vol. 14, no. 8, p. 1826, Apr. 2022.

[10] D. Wang, S. Liang, Y. Zhou, T. He, and Y. Yu, "A new method for retrieving daily land surface albedo from VIIRS data," *IEEE Trans. Geosci. Remote Sens.*, vol. 55, no. 3, pp. 1765–1775, Mar. 2017.

[11] X. Yin et al., "Significant discrepancies of land surface daily net radiation among ten remotely sensed and reanalysis products," *Int. J. Digit. Earth*, vol. 16, no. 1, pp. 3726–3753, 2023.

[12] S. Liang et al., "The global land surface satellite (GLASS) product suite," *Bull. Amer. Meteorol. Soc.*, vol. 102, no. 2, pp. E323–E337, Feb. 2021.

[13] D. Wang, S. Liang, T. He, and Q. Shi, "Estimation of daily surface shortwave net radiation from the combined MODIS data," *IEEE Trans. Geosci. Remote Sens.*, vol. 53, no. 10, pp. 5519–5529, Oct. 2015.

[14] J. Chen, T. He, B. Jiang, and S. Liang, "Estimation of all-sky all-wave daily net radiation at high latitudes from MODIS data," *Remote Sens. Environ.*, vol. 245, Aug. 2020, Art. no. 111842.

[15] S. Li et al., "Estimation of the all-wave all-sky land surface daily net radiation at mid-low latitudes from MODIS data based on ERA5 constraints," *Remote Sens.*, vol. 14, no. 1, p. 33, Dec. 2021.

[16] B. Bell et al., "The ERA5 global reanalysis: Preliminary extension to 1950," *Quart. J. Roy. Meteorol. Soc.*, vol. 147, no. 741, pp. 4186–4227, Oct. 2021.

[17] J. Xu, S. Liang, and B. Jiang, "A global long-term (1981–2019) daily land surface radiation budget product from AVHRR satellite data using a residual convolutional neural network," *Earth Syst. Sci. Data*, vol. 14, no. 5, pp. 2315–2341, May 2022.

[18] R. Gelaro et al., "The modern-era retrospective analysis for research and applications, version 2 (MERRA-2)," *J. Climate*, vol. 30, no. 3, pp. 5419–5454, Jul. 2017.

[19] H. Ma, S. Liang, Z. Xiao, and D. Wang, "Simultaneous estimation of multiple land-surface parameters from VIIRS optical-thermal data," *IEEE Geosci. Remote Sens. Lett.*, vol. 15, no. 1, pp. 156–160, Jan. 2018.

[20] X. Zhang et al., "An operational approach for generating the global land surface downward shortwave radiation product from MODIS data," *IEEE Trans. Geosci. Remote Sens.*, vol. 57, no. 7, pp. 4636–4650, Jul. 2019.

[21] Q. Liu et al., "Preliminary evaluation of the long-term GLASS albedo product," *Int. J. Digit. Earth*, vol. 6, no. 1, pp. 69–95, Dec. 2013.

[22] J. M. Sabater, *ERA5-Land Hourly Data From1950 to Present*. Copernicus Climate Change Service (C3S) Climate Data Store (CDS), 2019.

[23] J. Mu noz-Sabater et al., "ERA5-land: A state-of-the-art global reanalysis dataset for land applications," *Earth Syst. Sci. Data*, vol. 13, no. 9, pp. 4349–4383, Sep. 2021.

[24] H. Hersbach et al., "The ERA5 global reanalysis," *Quart. J. Roy. Meteorol. Soc.*, vol. 146, no. 730, pp. 1999–2049, Jul. 2020.

[25] Y. Zhang et al., "Generation of global 1 km daily soil moisture product from 2000 to 2020 using ensemble learning," *Earth Syst. Sci. Data*, vol. 15, no. 5, pp. 2055–2079, May 2023.